Received 8 September 2025; Accepted 17 October 2025
https://doi.org/10.48612/letters/2025-4-290-296
https://elibrary.ru/dhoooi

# Microstructure and mechanical properties of a novel low-activation austenitic steel after thermomechanical processing

I. Yu. Litovchenko†[1,2], S. A. Akkuzin[1], N. A. Polekhina[1], A. V. Kim[1,2], V. V. Osipova[1,2], K. V. Spiridonova[1], V. M. Chernov[3]

†litovchenko@ispms.ru

[1]Institute of Strength Physics and Materials Science of the Siberian Branch of the Russian Academy of Sciences, Tomsk 634055, Russia
[2]National Research Tomsk State University, Tomsk 634050, Russia
[3]A. A. Bochvar High-Technology Research Institute of Inorganic Materials, Moscow 123098, Russia

**Abstract:** This study investigates the microstructural characteristics of a novel low-activation chromium-manganese austenitic steel, Fe-11Cr-27Mn-W-Ti-V-Ta-Y-0.23C, following two processing routes: 20% cold rolling (CR) and high-temperature thermomechanical treatment (HTMT) involving 50% hot rolling deformation at 1100°C. HTMT resulted in the elongation of initially equiaxed grains along the rolling direction and their flattening within the rolling plane. The resulting microstructure comprised submicron and micron-sized fragments, predominantly bounded by low-angle misorientations. In contrast to the CR condition, which exhibited a high density of microtwins, the HTMT sample featured thinner, less dense twins and a dislocation density comparable to the quenched state. The temperature dependence of mechanical properties was evaluated from 20 to 700°C. The yield strength after CR was found to be 1.6 to 1.9 times higher than after HTMT across the entire temperature range. The minimum yield strength at 700°C was over 230 MPa for the HTMT condition and over 350 MPa for the CR condition. Conversely, the elongation to failure after HTMT was 1.4 to 2.6 times greater than that after CR. A minimum elongation of 11.8% was observed for the CR steel at 500 – 600°C, while the HTMT steel exhibited a minimum of 23.6% at 650°C. The discussion focuses on the influence of thermomechanical processing on the structural state, mechanical properties, the development of dynamic strain aging, and the underlying mechanisms of plastic deformation and fracture across the studied temperature range.

**Keywords:** low-activation austenitic steels, high-temperature thermomechanical treatment, microstructure, dislocation substructure, twins, carbides, mechanical properties, fracture

***Acknowledgements:*** *The study was funded by a grant of the Russian Science Foundation; Project No. 22-19-00802-P https://rscf.ru/project/22-19-00802/. The research was done using equipment of the Share Use Centre "Nanotech" of the Institute of Strength Physics and Materials Science SB RAS.*

## 1. Introduction

The induced activity of modern structural materials, particularly chromium-nickel austenitic steels, requires over 1000 years to decay to levels permitting safe handling after reactor decommissioning [1–3]. This prolonged radioactivity is primarily due to the presence of highly activating alloying elements such as Ni, Cu, Nb, Mo, Co, Al, and N. To mitigate the environmental impact of long-lived radioactive waste, the development of low-activation materials with minimized concentrations of these elements has become a critical research focus.

In response to this challenge, a new class of low-activation steels, including ferritic-martensitic and chromium-manganese austenitic grades, has been developed [1, 2, 4 – 8]. For these materials, the induced activity decays to a safe level within a significantly shorter period of 50 –100 years [3]. Despite this clear ecological advantage, the widespread adoption of low-activation steels has been hindered by several materials science challenges. For instance, earlier generations of low-activation chromium-manganese austenitic steels exhibited lower austenite stability compared to their chromium-nickel counterparts, demonstrating a greater tendency to transform into α′-martensite and δ-ferrite during processing or service [8 –12]. This phase instability is a significant concern, as it can accelerate swelling under irradiation compared to stable single-phase steels [7]. Furthermore, certain compositions are prone to the formation of brittle σ-phase during prolonged high-temperature aging or irradiation, which can lead to severe embrittlement [9 –13]. This precipitation is notably more prevalent in cold-worked states [12,13].

To date, the microstructure and mechanical properties of these steels have been extensively characterized in quenched and cold-deformed conditions, as well as after long-term aging and irradiation [4–17]. However, the influence of thermomechanical processing (TMP) on their behavior across a wide temperature range remains insufficiently explored. Such processing is of particular interest because the primary nucleation sites for $M_{23}C_6$ carbides (where M is Cr, Mn, Fe) during aging are grain boundaries, microtwin boundaries, and subboundaries [16,17]. A TMP regime designed to generate a high density of intragranular subboundaries could promote a more uniform dispersion of fine carbide precipitates within the grain interiors, thereby enhancing microstructural stability and mechanical properties.

The growing interest in these steels is further fueled by their potential application as non-magnetic structural materials in next-generation hybrid power plants. In our previous work, we have developed novel low-activation austenitic steels with enhanced phase stability and initiated studies on their thermal behavior during prolonged aging [14–18]. This paper builds upon that foundation by presenting a comprehensive study on the microstructure and mechanical properties of one such steel variant following specific thermomechanical treatments. We investigate the temperature dependence of strength and ductility from 20 to 700°C and discuss the underlying deformation and fracture mechanisms in the context of the induced microstructural states.

## 2. Materials and methods

For the studies, a novel low-activation austenitic steel, Fe-11Cr-27Mn-W-Ti-V-Ta-Y-0.23C [18] (Table 1), was selected in two structural states: after cold rolling (CR) and high-temperature thermomechanical treatment (HTMT). Multi-pass CR was performed after solution treatment at 1100°C for 1 hour followed by air cooling on a 2-roll mill at 20°C to a strain degree of $\varepsilon = 20\%$. The HTMT consisted of hot plastic deformation by rolling with heating up to 1100°C in a single pass to a strain degree of $\varepsilon = 50\%$ (the rolling mills were at room temperature). The actual temperature during deformation ranged approximately from 1000 to 900°C. After leaving the rolling mill, the samples were quenched in water.

The microstructure characterization was performed using an Apreo 2 S Scanning Electron Microscope (SEM) equipped with the energy dispersive X-ray (EDX) microanalysis system. The transmission electron microscopy (TEM) studies were carried out using thin foils on a JEOL JEM-2100 microscope (accelerating voltage 200 kV) equipped with an X-ray energy dispersive microanalysis system (EDX, Oxford Instruments INCA Energy). The SEM samples and thin foils for TEM examination were prepared by electropolishing in an electrolyte containing 450 ml of orthophosphoric acid and 50 g of chromic anhydride.

The mechanical tests were carried out by the method of static tensile deformation at a strain rate of $\approx 2\times10^{-3}$ s$^{-1}$ in the temperature range of 20–700°C (in air) on a MIM 2-50 testing machine using dog-bone samples with the gage length of 13 mm and the gage section of $2\times1$ mm$^2$. The samples were cut from the section parallel to the rolling plane and subjected to tension in the rolling direction. The fracture surfaces of the samples after the tensile tests were studied by the Apreo 2 S SEM.

## 3. Results

The microstructure of the Fe-11Cr-27Mn-W-Ti-V-Ta-Y-0.23C steel following CR has been detailed in the previous study [18]. Briefly, this state is characterized by a high density of deformation micro- and nanotwins, the presence of stacking faults and ε-martensite plates, and a significantly elevated dislocation density.

In contrast to the CR condition, the HTMT process resulted in a markedly different microstructure. SEM analysis revealed that the initially equiaxed grains became elongated along the rolling direction (Fig. 1a). The average grain size after HTMT was measured to be 47.7 μm, which is notably larger than that observed in the quenched state. Furthermore, plastic deformation was observed to develop heterogeneously, with localization within the grains.

Transmission electron microscopy (TEM) investigations confirmed the formation of a refined substructure (Fig. 1b–f). The original grains underwent fragmentation, resulting in a high density of submicron- and micron-sized subgrains. These fragments are predominantly bounded by low-angle misorientation boundaries. This is evidenced by analysis of selected area electron diffraction (SAED) patterns and dark-field (DF) images, which confirm that the misorientation angles between the fragments shown in Fig. 1d–f are low, typically below 10°.

In addition to the fragmented substructure with low-angle boundaries, the steel's microstructure after HTMT contained deformation twins, as shown in Fig. 2. These microtwins were observed both bordering regions of the fragmented structure and traversing through them. Notably, the twins formed during HTMT (Fig. 2c) are significantly thinner, with thicknesses on the order of tens of nanometers, and exhibit a considerably lower density than those observed in the CR condition [18].

Further TEM analysis (Fig. 3) revealed a non-uniformly distributed dislocation substructure with an overall high density, alongside finely dispersed MC-type carbide particles. Quantitative analysis using the linear intercept method [19] estimated the dislocation density to be in the range of approximately $(0.5-2)\times10^{15}$ m$^{-2}$. This value is comparable to that measured in the quenched state [18]. The key distinction lies in the arrangement: after HTMT, the dislocations are

**Table 1.** Elemental composition of a novel low-activation austenitic steel, Fe — base, wt.%.

| Cr | Mn | Ni | Cu | W | V | Ti | Ta | Y | B |
|---|---|---|---|---|---|---|---|---|---|
| 10.6 | 26.6 | 0.04 | 0.05 | 0.48 | 0.065 | 0.075 | 0.06 | 0.01 | 0.006 |
| Nb | Mo | Co | Al | Si | S | P | C | N | O |
| 0.01 | 0.013 | 0.05 | 0.04 | 0.65 | 0.0035 | 0.009 | 0.226 | 0.0164 | 0.0005 |

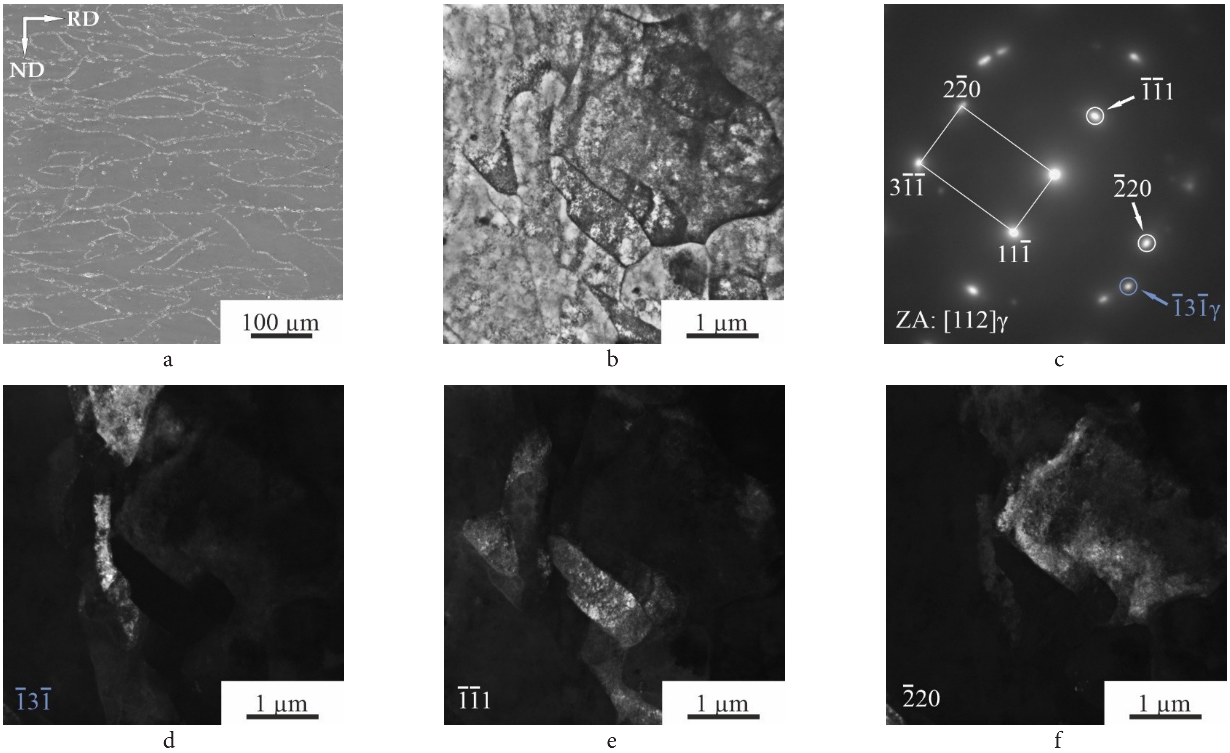


**Fig. 1.** Microstructure of steel after HTMT. SEM image in secondary electrons (a), TEM Bright-field (BF) image of fragmented structure (b), selected area electron diffraction (SAED) pattern from Fig. 1b (c), Dark-field (DF) images in the reflections marked up on Fig. 1c (d – f).

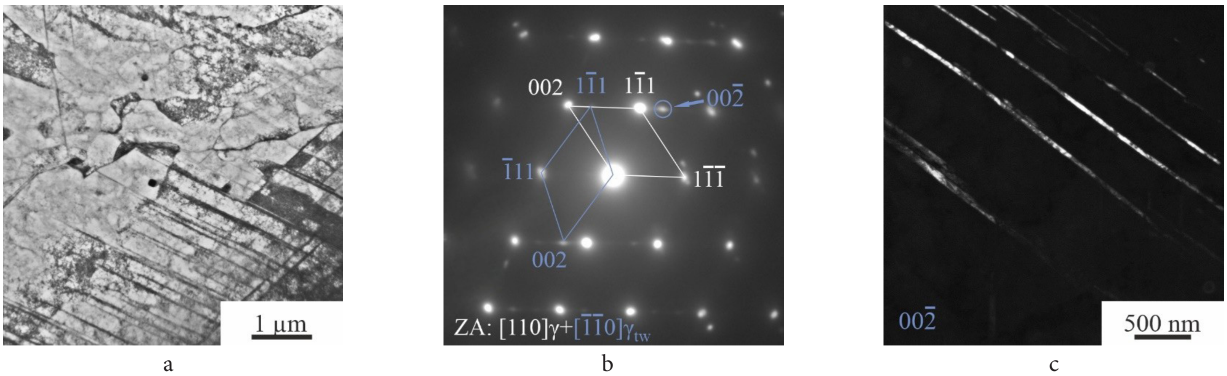


**Fig. 2.** TEM images after HTMT. (BF) image of fragmented and twinned structure (a), SAED pattern from twins (b), Magnified DF image in the twin reflection (d).

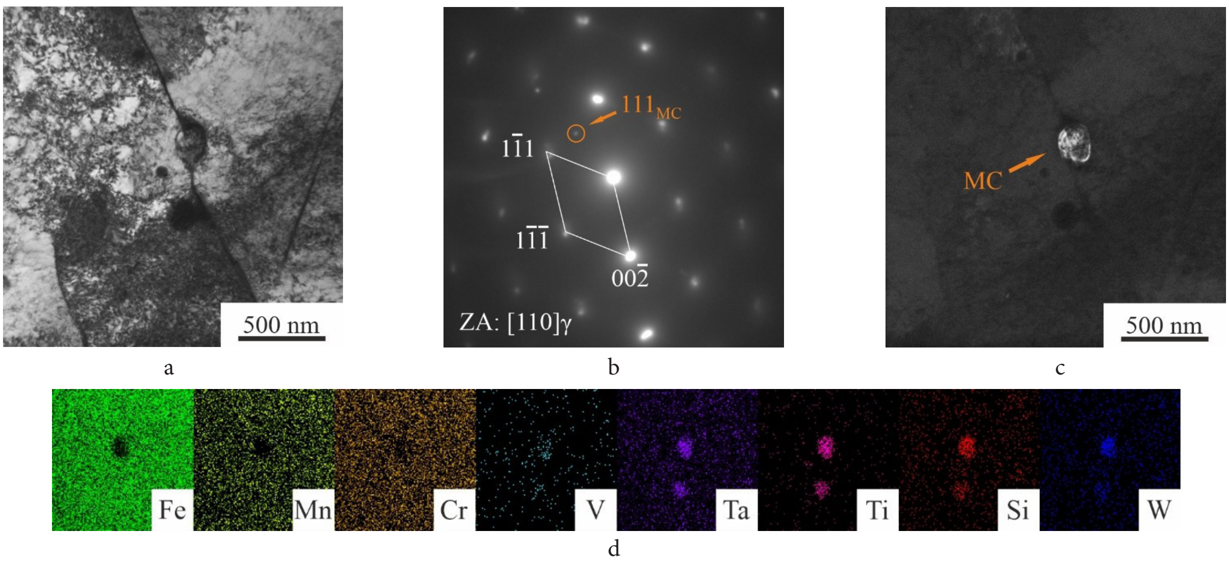


**Fig. 3.** (Color online) TEM images after HTMT. (BF) image of fragmented structure with MC particles (a), SAED pattern from Fig. 3 a (b), DF image in the reflection of MC particle (c), corresponding elemental map (d).

organized into the observed substructure rather than being randomly distributed.

Energy-dispersive X-ray spectroscopy identified the submicron MC-type particles as being enriched with Ti, V, Ta, Si, and W (Fig. 3d). These particles are consistent with those previously observed in both the quenched and CR states of this steel [18]. This indicates that the HTMT process did not induce the precipitation of new MC carbides beyond those already present from quenching. Furthermore, a critical finding was the absence of coarse $M_{23}C_6$ carbide particles, which are typically found in the quenched and CR states [18], following the HTMT process.

The engineering stress-strain curves for the steel following both CR and HTMT, obtained from tensile tests conducted between 20 and 700°C, are presented in Fig. 4. The temperature dependencies of the mechanical properties, derived from multiple samples tested at each temperature, are summarized in Fig. 5. Analysis of the data reveals a significant strength advantage for the CR condition. The yield strength (YS) and ultimate tensile strength (UTS) after CR exceed those after HTMT by factors of 1.6–1.9 and 1.1–1.4, respectively, across the entire temperature range. This strength differential persists even at elevated temperatures, with the minimum YS at 700°C measured at over 350 MPa for the CR state, compared to over 230 MPa for the HTMT state. Conversely, the HTMT state exhibits superior ductility. The elongation to failure (δ) after HTMT is 1.4 to 2.6 times greater than the corresponding values after CR. When compared to the previously reported quenched state [18], the HTMT condition offers a favorable balance: it provides higher strength properties but lower ductility. A notable characteristic of the HTMT state is the considerable scatter in elongation to failure values (Fig. 5b). This scatter in the data can be explained by the microstructural heterogeneity resulting from HTMT, specifically the non-uniform distribution of dislocation substructures.

An increase in tensile test temperature results in a decrease in both the yield strength and ultimate tensile strength for the steel in both the CR and HTMT conditions. The most pronounced strength reduction occurs at temperatures exceeding 600°C. This is evident for the YS and UTS after CR, as well as for the UTS after HTMT. In contrast, the YS after HTMT demonstrates the highest thermal stability, with the smallest reduction (approximately 100 MPa) observed between 600 and 700°C. The elongation to failure exhibits a non-monotonic dependence on temperature within the 400–700°C range. Minimum ductility values are observed at 500–600°C for the CR state (11.8%) and at 500–650°C for the HTMT state (above 23%). This ductility drop coincides with the appearance of serrated flow on the tensile curves of the HTMT-treated steel, a hallmark of the Portevin-Le Chatelier effect. The reduction in ductility and the serrated

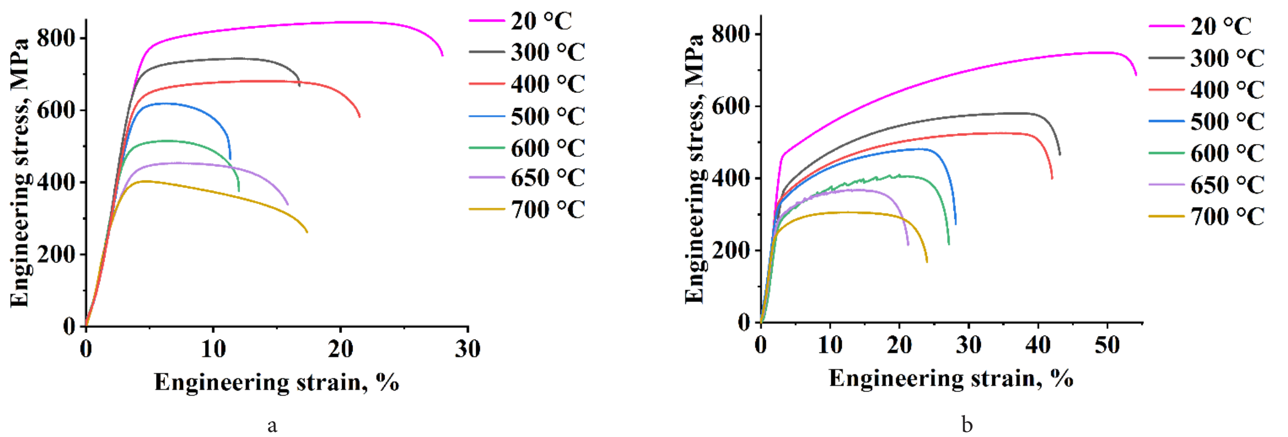


**Fig. 4.** (Color online) Engineering stress-strain curves after CR (a) and HTMT (b).

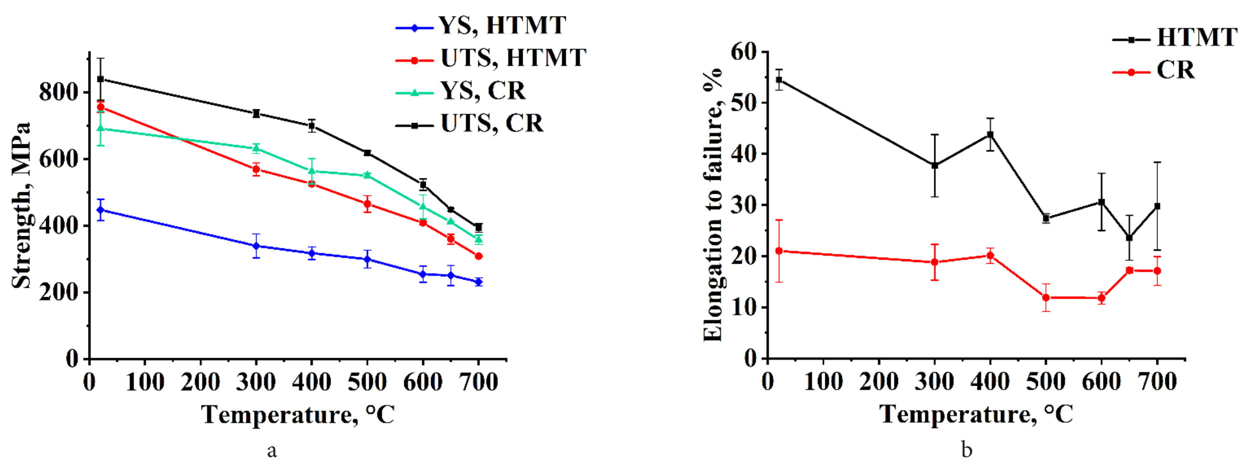


**Fig. 5.** (Color online) Mechanical properties of steel after CR and HTMT vs temperature. Yield strength (YS) and ultimate tensile strength (UTS) (a), elongation to failure (b).

flow are characteristic manifestations of dynamic strain aging (DSA) [15,20]. The DSA mechanism involves the repeated pinning of mobile dislocations by diffusing solute atoms (e.g., C, N) and their subsequent unpinning, which leads to the characteristic serrations on the stress-strain curves and a consequent decrease in uniform elongation. At higher deformation temperature (700°C) the tendency for dislocation climb increases, making them more easy to tear off from obstacles and leading to increased ductility [15].

Prior research has detailed the fracture mechanisms of the low-activation austenitic steel Fe-11Cr-27Mn-W-Ti-V-Ta-Y-0.23C in the quenched and CR conditions at 20, 650, and 700°C [18]. A key finding was that the quenched state exhibited a mixed fracture mode at 20°C, comprising primarily ductile transgranular dimple rupture alongside elements of ductile intergranular fracture. The cold rolling process markedly suppressed intergranular fracture. The present study demonstrates that HTMT further enhances the fracture mode. As shown in Fig. 6, HTMT promotes the almost complete elimination of ductile intergranular fracture elements. Following this treatment, fracture occurs exclusively via a ductile transgranular dimple mechanism across all tested temperatures. At room temperature (20°C), microscopic analysis reveals only minor incipient cracking along grain boundaries, representing the initial stages of ductile void formation (Fig. 6d). At elevated temperatures (650 and 700°C), even these minor intergranular features are absent. Furthermore, the average dimple size increases significantly to several tens of microns, indicating enhanced microvoid coalescence and greater overall ductility at high temperatures (Fig. 6e,f).

## 4. Discussion

The intense mechanical twinning observed under CR conditions is a direct consequence of the relatively low stacking fault energy (SFE) of steel, approximately 26.4 mJ/m² [18]. However, SFE is known to increase with temperature [21]. Thermodynamic modeling using the JMatPro software [22] estimates the SFE to be in the range of 170–180 mJ/m² at the actual HTMT deformation temperatures of 900–1000°C. At these significantly higher SFE values, mechanical twinning is suppressed, and dislocation slip becomes the predominant deformation mechanism. This transition in deformation mechanisms with increasing temperature is a well-documented phenomenon in austenitic steels [20,23]. The dominance of dislocation slip facilitates the formation of the observed fragmented substructure with low-angle misorientation boundaries within the grains (Figs. 1–3). The development of this substructure is likely accompanied by intensive dynamic recovery processes. This is supported by the measured dislocation density after HTMT, which, despite the extensive deformation, is comparable to that of the quenched state (on the order of $(0.5-2)\times10^{15}$ $m^{-2}$). The subsequent rapid cooling (quenching) from the deformation temperature introduces quench stresses. It is proposed that these stresses are responsible for the formation of the limited number of thin microtwin plates observed after HTMT. An important finding is the absence of coarse $M_{23}C_6$ carbide particles following HTMT. This suggests that the hot deformation process may have promoted the dissolution of such carbides that were present after prior quenching. Furthermore, the high density of intragranular subboundaries introduced by HTMT is expected to significantly alter the precipitation behavior during subsequent high-temperature exposure. This refined substructure could shift the preferred nucleation sites for $M_{23}C_6$ particles from grain and twin boundaries to these intragranular dislocations and subboundaries, thereby potentially enhancing microstructural stability and influencing the overall kinetics of precipitation.

A comparison of the mechanical properties reveals that the HTMT condition results in an intermediate balance of strength and ductility, situated between the quenched [18] and CR states. This can be attributed to the distinct microstructural features induced by each processing route.

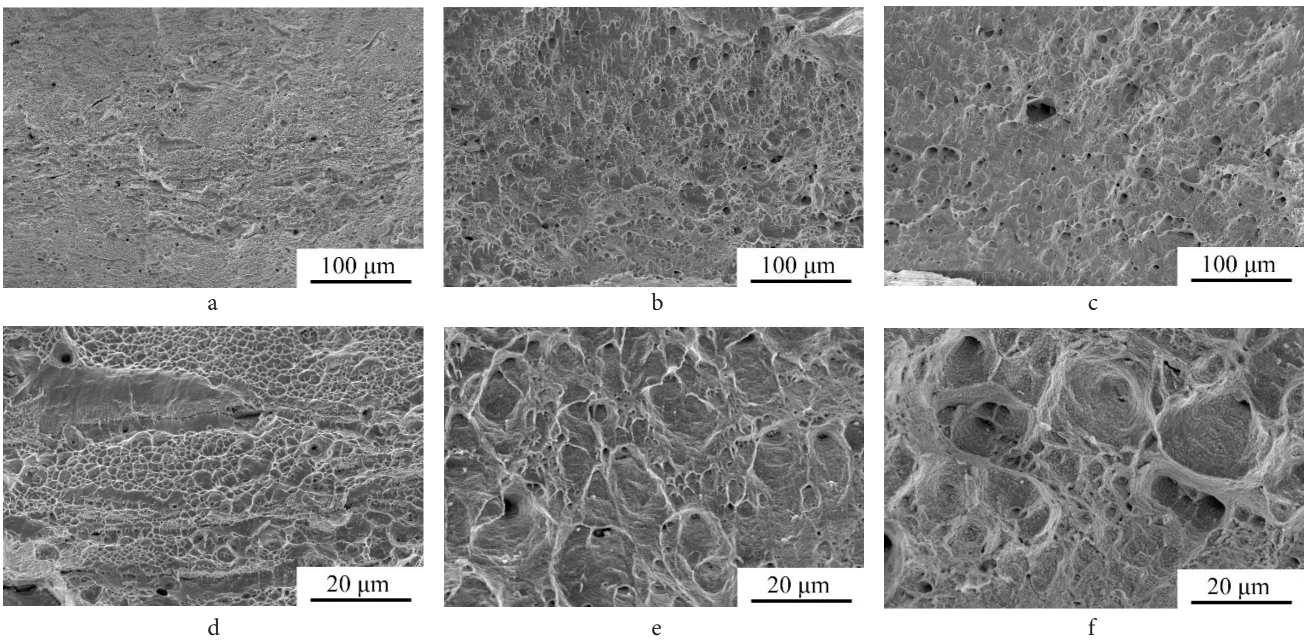


**Fig. 6.** Fractographic images of steel after HTMT, broken at different temperatures: 20°C (a,d); 650°C (b,e); 700°C (c,f).

The fragmented dislocation substructure formed during HTMT provides effective strengthening relative to the quenched state, leading to higher strength but moderately reduced ductility. This strengthening arises from the increased density of low-angle boundaries and dislocations, which impede dislocation glide. In contrast, the CR state exhibits the highest strength but the lowest ductility. This is a direct consequence of the high density of deformation microtwins and the associated elevated dislocation density, which create a potent strengthening effect but provide limited capacity for uniform plastic deformation, promoting earlier fracture. The HTMT process, by suppressing extensive twinning and promoting a more recoverable dislocation substructure, achieves a superior compromise between these competing properties. The absence of coarse brittle phases and the prevalence of a ductile dimple fracture mode further contribute to the enhanced ductility of the HTMT-treated steel.

The distinct structural states produced by CR and HTMT govern the plastic deformation behavior of the steel across the studied temperature range. A key observation is the manifestation of dynamic strain aging, evidenced by serrated flow on the tensile curves, in the steel after both HTMT (Fig. 4b) and in the previously reported quenched state [18]. In contrast, DSA is suppressed after CR, as indicated by the absence of serrations on the corresponding flow curves (Fig. 4a). This inhibition is likely attributable to the high density of deformation twins, which constitute special types of high-angle boundaries introduced by severe cold work. This finding is consistent with the literature [20], where a high density of high-angle boundaries has been shown to suppress DSA. These boundaries act as potent obstacles, immobilizing dislocations and thereby hindering the repetitive pinning-unpinning process between dislocations and solute atoms that is fundamental to the DSA phenomenon.

Ductile intergranular fracture, which is characteristic of the quenched state and remains partially after CR [18], is nearly completely suppressed at 20°C by the microstructure produced by HTMT. This significant improvement in fracture mode is likely a consequence of the well-developed dislocation substructure and the associated enhancement of intragranular strength. In the quenched state, the relative softness of the grain interiors promotes localized plastic deformation and stress concentration at grain boundaries during tensile testing. This stress concentration facilitates void nucleation and coalescence along grain boundaries, leading to the observed ductile intergranular fracture. The HTMT process mitigates this mechanism through microstructural refinement. The increased density of intragranular obstacles (dislocation subboundaries) and, to a lesser extent, deformation twins strengthens the grain interiors more uniformly. This homogeneous intragranular strengthening reduces the strain partitioning between the grain boundaries and the matrix, minimizes stress concentration at boundaries, and promotes transgranular void formation. Consequently, the fracture mode shifts entirely to a ductile dimple fracture within the grains, suppressing the undesirable intergranular failure.

## 5. Conclusions

This study investigated the effect of high-temperature thermomechanical treatment on the microstructure and mechanical properties of a novel low-activation austenitic steel. The key findings are summarized as follows:

1. HTMT via hot rolling resulted in significant microstructural refinement. The initially equiaxed grains were elongated and flattened, forming a substructure of micron- and submicron-sized fragments bounded predominantly by low-angle misorientation boundaries. This treatment also suppressed the formation of deformation twins and coarse $M_{23}C_6$ carbides, resulting in a twin density and thickness significantly lower than those observed after cold rolling.

2. The mechanical properties of the steel after HTMT represent an optimal balance between the quenched and CR states across the 20 – 700°C temperature range. The yield and tensile strengths are lower than those after CR but higher than after quenching. Conversely, the ductility (elongation to failure) is superior to that of the CR state yet lower than that of the quenched state.

3. Dynamic strain aging is observed in the HTMT and quenched conditions but is suppressed after CR. This inhibition is attributed to the high density of deformation twins (high-angle boundaries) introduced by CR, which immobilize dislocations and prevent the characteristic pinning-unpinning mechanism of DSA.

4. The well-developed dislocation substructure after HTMT enhances intragranular strength, leading to a near-complete elimination of ductile intergranular fracture elements at room temperature. This represents a significant improvement over the fracture modes characteristic of the quenched and CR states.

5. The refined substructure produced by HTMT is anticipated to alter the precipitation behavior of $M_{23}C_6$ carbides during prolonged high-temperature aging. The high density of intragranular defects is expected to shift the preferred nucleation sites from grain boundaries to dislocation substructures, thereby potentially influencing the kinetics and distribution of precipitates and improving microstructural stability.

## References


1. L. I. Ivanov, Yu. M. Platov, Radiation Physics of Metals and Its Applications 2nd Edition, Cambridge International Science Publishing, Cambridge, 2004, 356 p.
2. Y. Pascal, Structural Materials for Generation IV Nuclear Reactors, Woodhead Publishing Series in Energy: Number 106, Kindle Edition, 2020, p. 644.
3. A. I. Blokhin, V. M. Chernov, Nuclear Physical Properties of Austenitic Nickel and Manganese Steels under Neutron Irradiation in Nuclear Fission (Fast) and Fusion Reactors. Phys. At. Nucl. 84, 7 (2021) 1272 – 1284.
4. R. L. Klueh, P. J. Maziasz, Tensile and microstructural behavior of solute-modified manganese-stabilized austenitic steels, Mater. Sci. Eng. A 127 (1990) 17 – 31.
5. M. Onozuka, T. Saida, S. Hirai, M. Kusuhashi, I. Sato, T. Hatakeyama, Low-activation Mn-Cr austenitic

stainless steel with further reduced content of long-lived radioactive elements, J. Nucl. Mater. 255 (1998) 128–138.
6. Y. Suzuki, T. Saida, F. Kudough, Low activation austenitic Mn-steel for in-vessel fusion materials, J. Nucl. Mater. 258 (1998) 1687–1693.
7. E.V. Demina, M.D. Prusakova, V.V. Roshchin, N.A. Vinogradova, G.D. Orlova, Reduced activation Fe-Cr-Mn austenitic steels for nuclear power plants, Inorg. Mater.: Applied Research 1 (2010) 115–124.
8. R.L. Klueh, P.J. Maziasz, E.H. Lee, Manganese as an austenite stabilizer in Fe-Cr-Mn-C steels, Mater. Sci. Eng. A 102 (1988) 115–124.
9. K. Miyahara, F.A. Garner, Y. Hosoi, Microstructures of neutron-irradiated Fe-12Cr-*X*Mn ($X$=15–30) ternary alloys, J. Nucl. Mater. 191–194 (1992) 1198–1203.
10. S. Ohnuki, F.A. Garner, H. Takahashi, Phase instability and void formation neutron-irradiated Fe-Cr-Mn-Ni alloys, Mater. Trans. JIM 34 (1993) 1031–1035.
11. J.I. Cole, D.S. Gelles, J.J. Hoyt, Phase stability of reduced-activation Mn-stabilized austenitic steels J. Nucl. Mater. 191–194 (1992) 657–661.
12. F.A. Garner, F. Abe, T. Noda, Response of Fe-Cr-Mn austenitic alloys to thermal aging and neutron irradiation, J. Nucl. Mater. 155–157 (1988) 870–876.
13. F. Abe, H. Araki, T. Noda, Discontinuous precipitation of σ-phase during recrystallization in cold rolled Fe-10Cr-30Mn austenite, Mater. Sci. Tech. 4 (1988) 885–893.
14. I. Litovchenko, S. Akkuzin, N. Polekhina, K. Almaeva, V. Linnik, A. Kim, E. Moskvichev, V. Chernov, The microstructure and tensile properties of new high-manganese low-activation austenitic steel, Metals 12 (2022) 2106.
15. I. Litovchenko, S. Akkuzin, N. Polekhina, K. Spiridonova, V. Osipova, A. Kim, E. Moskvichev, V. Chernov, A. Kuznetsov, Microstructure Features and Mechanical Properties of Modified Low-Activation Austenitic Steel in the Temperature Range of 20 to 750°C, Metals 13 (12) (2023) 2015.
16. I. Litovchenko, S. Akkuzin, N. Polekhina, K. Spiridonova, V. Osipova, A. Kim, E. Moskvichev, V. Chernov, Effect of aging at 700°C on the microstructure, phase transformations, and mechanical properties of low-activation austenitic steel, Materialia 39 (2025) 102335.
17. I. Litovchenko, S. Akkuzin, N. Polekhina, K. Spiridonova, V. Osipova, Phase transformations in low-activation chromium-manganese austenitic steel under long-term aging, Met. Sci. Heat Treat. 67 (2025) 89–98.
18. I.Y. Litovchenko, S.A. Akkuzin, N.A. Polekhina, K.V. Spiridonova, A.V. Kim, V.V. Osipova, E.N. Moskvichev, V.M. Chernov, Microstructure and mechanical properties of Y-modified low-activation austenitic steel, Lett. Mater. 14 (2024) 346–352.
19. J. Gallet, M. Perez, R. Guillou, C. Ernould, C. Le Bourlot, C. Langlois, B. Beausir, E. Bouzy, T. Chaise, S. Cazottes, Experimental measurement of dislocation density in metallic materials: a quantitative comparison between measurements techniques (XRD, R-ECCI, HR-EBSD, TEM), Mater. Charact. 199 (2023) 112842.
20. S. Akkuzin, I. Litovchenko, N. Polekhina, K. Almaeva, A. Kim, E. Moskvichev, V. Chernov, Effect of multistage high temperature thermomechanical treatment on the microstructure and mechanical properties of austenitic reactor steel, Metals 12 (2022) 63.
21. T.H. Lee, H.Y. Ha, B. Hwang, S.-J. Kim, E. Shin, Effect of carbon fraction on stacking fault energy of austenitic stainless steels, Metallurg. Mater. Trans. A 43 (2012) 4455–4459.
22. JMatPro. Practical software for materials properties: Available online (accessed on 2021).
23. S. Akkuzin, I. Litovchenko, N. Polekhina, A. Kim, K. Spiridonova, E. Moskvichev, Effect of multi-pass warm rolling and annealing on microstructure and mechanical properties of an austenitic steel, J. Mater. Eng. Perf. (2025).